ELSEVIER

Polymer 44 (2003) 2441–2446

polymer

www.elsevier.com/locate/polymer

Effect of sample thickness on the mechanical properties of injection-molded polyamide-6 and polyamide-6 clay nanocomposites

Paola Uribe-Arocha[a,*], Christof Mehler[b,1], Judit E. Puskas[c,2], Volker Altstädt[a,3]

[a]*Department of Polymer Materials, University Bayreuth, FAN A/Universitätstraße 30, D95447 Bayreuth, Germany*
[b]*BASF AG, Polymer Laboratory, D67056 Ludwigshafen, Germany*
[c]*Department of Chemical and Biochemical Engineering, The University of Western Ontario, London, Ont., Canada N6A 5B9*

Received 29 August 2002; received in revised form 9 January 2003; accepted 28 January 2003

Abstract

The effect of the thickness on the mechanical properties of injection-molded specimens of pure polyamide-6 (PA6) and polyamide-6 clay nanocomposites (PA6-NC) with 5 wt% of layered silicates was investigated. Plates of 0.5, 0.75, 1 and 2 mm thickness were characterized in the injection direction using Dynamic Mechanical Analysis under torsion and tension respectively, and tensile tests. The fracture surfaces were analyzed by Scanning Electron Microscopy. In contrast with PA6, PA6-NC showed thickness effect and clear differences in the mechanical and thermomechanical properties between skin and core, especially in the 2 mm thick samples. Increasing thickness in PA6-NC led to a reduction of tensile modulus and yield stress. In the fracture surface of the thicker tensile specimens the formation of a sheet-like structure was observed. Multiple voiding in the core causing initial failure in this region and a stiffer skin with a better orientation of the layered silicates in the injection direction are two important elements of a micromechanical model proposed in this paper to explain the fracture mechanism in PA6-NC.

Keywords: Polyamide-6 nanocomposites; Injection molding; Mechanical properties

1. Introduction

The production of polyamide (PA) nanocomposites using layered silicates as reinforcing agents has thoroughly been investigated during the last decade. The first step is the hydrophobation and swelling of the layered silicates with alkylammonium salts, which replace the Na^+ ions between the silica layers (cation exchange). This will allow intercalation or delamination of the clays [1–5] by increasing the interlayer spacing, improving compatibility with the polymer. The clay is then used to prepare nanocomposites using mainly in situ polymerization [6,7] or melt intercalation [8–12]. In this latter method, the organophilic clay is mixed with the polymer melt (for example, in an extruder), so the shear forces will delaminate the clay into nanometer-sized individual silicate platelets.

The interaction between the layered silicates and the polymer in nanocomposites leads to improved properties, e.g. lower gas permeability [13], better thermal stability and flame retardancy [13–16], better tensile and impact strength, stiffness and fatigue [17–20], compared to the unmodified polymer. The layered silicates were shown to orient along the direction of shear, causing orientation of the polymer chains as well [21]. The ratio of the α/γ PA crystal structures was found to be dependent on the layered silicate content [22], with the γ crystal structure with extended polymer chains positioned mostly close to the oriented silicate/polymer interface. It was also found that thermal history, such as annealing after injection molding, had a dramatic effect on α/γ crystal structure ratio (fraction of α phase increases from 1/3 to 2/3 after annealing) [23]. It may be foreseen that α/γ ratios and orientation would be affected by processing parameters. For instance, during injection molding thinner samples experience more uniform shear distribution and faster cooling than thicker ones, which would influence the crystal structure and

* Corresponding author. Tel.: +49-921-55-7482; fax: +49-921-55-7473.
E-mail addresses: paola.uribe@uni-bayreuth.de (P. Uribe-Arocha), christof.mehler@basf-ag.de (C. Mehler), jpuskas@uwo.ca (J.E. Puskas), altstaedt@uni-bayreuth.de (V. Altstädt).
[1] Tel.: +49-621-60-22531; fax: +49-621-60-20313.
[2] Tel.: +1-519-661-4184; fax: +1-519-850-2343.
[3] Tel.: +49-921-55-7470; fax: +49-921-55-7473.

0032-3861/03/$ - see front matter © 2003 Elsevier Science Ltd. All rights reserved.
doi:10.1016/S0032-3861(03)00115-0

orientation. Indeed, crystallinity in the core of injection-molded PA specimens increased dramatically (from 18 to 30%) with sample thickness, while remaining nearly constant at about 15% in the skin [24]. Investigations into the effects of processing conditions in fiber-reinforced thermoplastics [25–29] also revealed the formation of a skin-core structure in injection-molded short-glass fiber reinforced PA6. This is caused by shear-induced orientation and is influenced by many parameters such as temperature, shear forces in the tool, thickness of the tool, geometry of the tool, etc [30]. The effects of processing conditions on PA6-NC have not been investigated in detail, except for data published in Ref. [24]. In this study much higher crystallinity was found in thin specimens or in the skin of thicker specimens. The same study showed that in PA6-NC crystallinity decreased with increasing specimen thickness, both in the skin and core, with somewhat higher crystallinity in the skin.

It is clear that more detailed investigations into the effects of processing conditions on the properties of PA6-NC composites are warranted. This work will investigate the mechanical properties and fracture mechanism of injection-molded PA6 and PA6-NC plates of varying thickness.

2. Experimental

2.1. Materials

Commercial PA6 (Ultramid B3) was supplied by BASF AG (Ludwigshafen, Germany). Cloisite 30B (Southern Clay Products, Inc.) a commercial organoclay (montmorillonite) modified with methyl tallow bis-2-hydroxyethyl quaternary ammonium chloride was used as reinforcement material for the fabrication of the PA6-NC.

2.2. Preparation of polyamide-6 clay nanocomposites

PA6-NC was produced with melt intercalation in a double screw extruder (250 rpm, 20 kg/h, 250 °C). Unmodified PA6 was submitted to identical processing conditions to ensure similar thermomechanical history.

2.3. Preparation of injection-molded plates

PA6 and PA6-NC were injection-molded into 110 mm × 110 mm plates with 0.5, 0.75, 1 and 2 mm thickness in a Kraus Maffei KM 250/900 B injection molding machine (cylinder temperature 260–280 °C; tool temperature 100 °C; 30 °C for the 2 mm plates; 100 rpm, 95 mm/s).

2.4. Dynamic Mechanical Analysis (DMA)

All samples were dried at 75 °C for 48 h in a vacuum oven prior to DMA measurements. Dynamic temperature sweep measurements in torsion were performed using 1 Hz frequency, a temperature interval of 30–330 °C with a heating rate of 3 °C/min, 0.1% strain (0.4% for the 0.5 mm samples), 0.001–0.1 N torque. Specimens with dimensions of 10 mm × 40 mm were machined from the injection-molded plates in the injection direction using a Diadisc 6200 (Mutronic) cutter; the edges and surface quality was improved by grinding.

DMA measurements in tension were performed using a Rheometrics Solids Analyzer (RSA II) using the same frequency, temperature interval and heating rate as in torsion, applying 0.02–0.025% strain and an initial static force of 0.49–0.83 N. The specimen size in this test was 6 mm × 40 mm, cut from the injection-molded plates in the injection direction. It should be noted that the 2 mm thick samples could not be tested with the RSAII because of limited grid size (max 1.5 mm).

2.5. Tensile tests

Standard dumbbell specimens (5A, DIN EN ISO 527-2: 1996-07) were cut from the injection-molded plates parallel to the injection molding direction. All samples were dried at 75 °C for 48 h in a vacuum oven prior to the measurements.

Tensile tests were performed using a Universal Testing Machine (Zwick 1455) at 22 °C and 64–66% relative humidity, with a 20 mm initial grid distance, 0.5 N initial load, and a crosshead speed of 5 mm/min.

2.6. Scanning Electron Microscopy (SEM)

SEM studies of the fracture surface of the tensile specimens were carried out with a JEOL JSM IC 848 instrument (15 kV, 6×10^{-11} A). The surfaces were gold-coated prior to the measurements.

Special 0.75 mm thick samples were additionally prepared from the original 2 mm thick specimens by removing the skin; equal amounts of mass from both sides were grinded down. They were then submitted to the same tensional load as specified in the tensile tests, and the obtained fracture surfaces were compared with those of the original skin-core samples. To avoid confusion with the injection-molded 0.75 mm samples, these samples will be marked ‘core samples’.

3. Results and discussion

DMA under torsion and tension was used to analyze the samples whether skin-core structure can be identified. Under torsion mostly the outer part or skin of the test specimen is loaded,[4] while under tension the total cross-section of the sample contributes to the modulus.

[4] Assuming that the effects caused by the corners of the squared samples can be neglected, the behavior of the load across the thickness would be similar as the one present in a cylindrical specimen. Under torsion a shear stress is generated. This parameter reaches the highest value in the outer part of the specimen and decreases linearly when approaching the center, where its value is equal to zero [31].

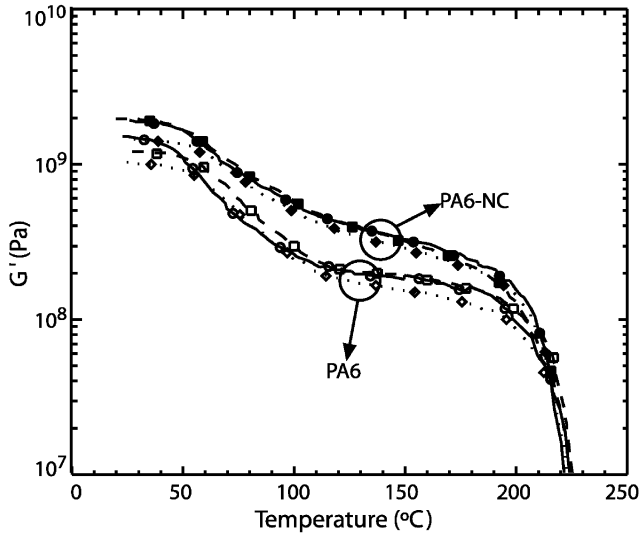

Fig. 1. DMA in torsion. Storage modulus G' values as a function of temperature. PA6: —○— 0.5 mm; –□– 0.75 mm; ···◇··· 1 mm. PA6-NC: —●— 0.5 mm; –■– 0.75 mm; ···◆··· 1 mm.

In Fig. 1 storage moduli data under torsion (G') vs. temperature plots for both PA6 and PA6-NC specimens are represented. In the entire temperature range the PA6-NC samples have higher moduli with less drop at T_g than the PA-6 samples. The T_g onset values of 50 °C are independent on sample type and thickness. No clear thickness effect can be identified in either PA6-NC or PA6.

In tension, the effect of sample thickness on the moduli values is clearly evident in the case of the nanocomposites, as shown in Fig. 2. Thinner samples had higher storage moduli, thus higher stiffness. This points to higher degree of orientation near the wall of the tool. This would translate into the existence of a highly oriented skin and less oriented core in thicker samples. This is consistent with a decreasing degree of

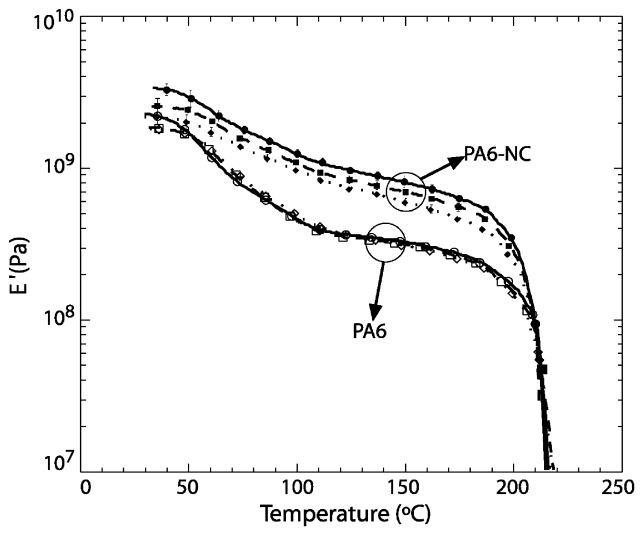

Fig. 2. DMA in tension. Storage modulus E' as a function of temperature. PA6: —○— 0.5 mm; –□– 0.75 mm; ···◇··· 1 mm. PA6-NC: —●— 0.5 mm; –■– 0.75 mm; ···◆··· 1 mm.

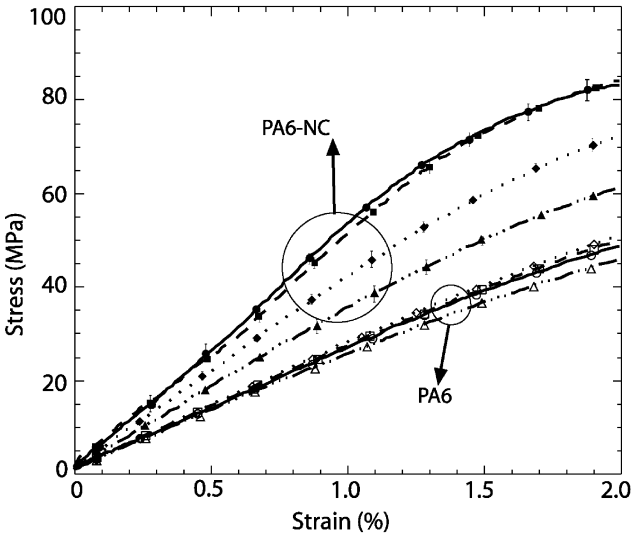

Fig. 3. Stress–strain curves of PA6 and PA6-NC in the low-strain region (0.0–2.0% strain). PA6: —○— 0.5 mm; –□– 0.75 mm; ···◇··· 1 mm; —△··· 2 mm. PA6-NC: —●— 0.5 mm; –■– 0.75 mm; ···◆··· 1 mm; —▲··· 2 mm.

crystallinity with sample thickness, and higher crystallinity in the core shown in Ref. [24]. In contrast to that reported in Ref. [24], no skin effect was identified in PA6 specimens in our studies.

Tensile test data are summarized in Table 1. Fig. 3 shows the stress–strain curves at low strain (0–2.0%). The plots of the PA6 samples run close to each other, while in PA6-NC the Young Moduli decrease significantly with increasing thickness. This is again most likely due to higher degree of orientation in the thinner samples in the direction of the tensional load (more skin), compared to the thicker samples (more core). Fig. 4 shows full stress–strain plots. Both PA6 and PA6-NC show yielding, but the strain to failure is considerably lower for the nanocomposites. In the 2 mm thick PA6-NC the stress decreases until failure, at approximately 40% strain.

The reinforcing effect of the layered silicates observed in the G' and E' (see Figs. 1 and 2) is also evident from the tensile curves: higher tensile strength and stiffness and reduction of the strain to failure is observed in the nanocomposites (Figs. 3 and 4).

Fig. 5 shows the SEM picture of the side view of a failed 2 mm thick PA6-NC specimen. Formation of voids within the core is apparent from the picture (voids indicated with black arrows in the figure). These voids were observed with all 2 mm thick PA6-NC samples.

Fig. 6 presents SEM pictures of the fracture surfaces of selected tensile specimens. The thin (0.5 mm) samples of both PA6 and PA6-NC show similar flat fracture surfaces, reflecting fast crack propagation when failure occurs. In contrast, in the thicker samples, especially in the 2 mm ones, while the fracture surface of PA6 remains flat, PA6-NC shows a sheet-like pattern in the core and a smoother surface in the skin. We theorize that this sheet-like pattern can only

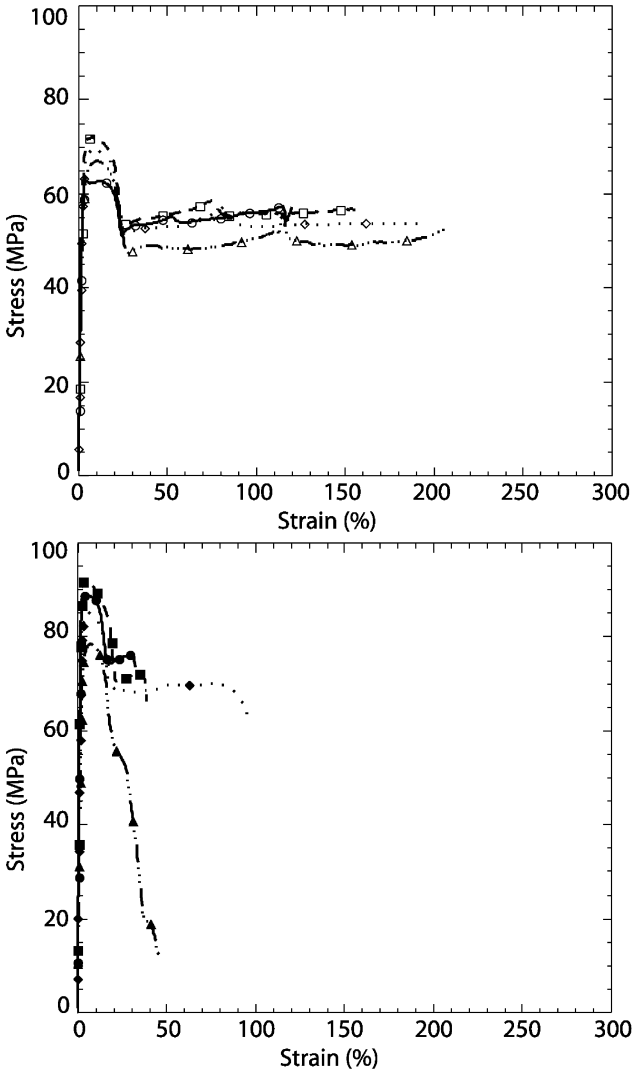

Fig. 4. Stress–strain curves of PA6 and PA6-NC. PA6: —○— 0.5 mm; –□– 0.75 mm; ···◇··· 1 mm; —△··· 2 mm. PA6-NC: —●— 0.5 mm; –■– 0.75 mm; ···◆··· 1 mm; —▲··· 2 mm.

be formed, if both skin and core are present. In the micrograph of the core sample manufactured from the 2 mm thick specimens (see Section 2) for example, only the formation of large cracks in the center of the sample can be seen. In this core sample sheeting did not develop because

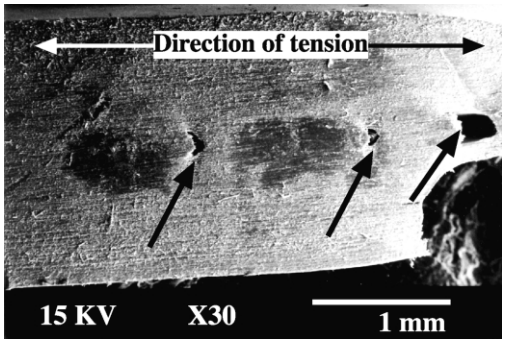

Fig. 5. SEM micrograph of the side of a PA6-NC tensile test specimen.

the skin was removed so the tear effect caused by the skin in the thick samples is missing.

Based on the results discussed above, the model presented in Fig. 7 to describe the failure mechanism in PA6-NC is proposed. The probable starting platelets orientation in the specimen is also represented, exaggerating the sizes of the platelets for a better view. This orientation is based on the assumption of a parabolic velocity distribution across the thickness of the mold, generated during the injection molding process. During fracture, the stress concentration is the highest in the core, where the orientation in the load direction is lower. Therefore cracks appear first in the core. The skin is stiffer than the core, having a better orientation in the load direction. This gives the skin the ability to sustain higher load and to deform more than the core, facilitating void formation and growth in the core. The voids grow in the load direction and multiply until the core fails completely. Thus a sheet-like structure develops in the core, elongating more until a sudden breakage occurs.

The model proposed above explains the different fracture behavior of thin and thick PA6-NC. More investigations are underway in our laboratory.

4. Conclusions

From the injection-molded PA6-NC samples examined in this work a thickness effect could be observed using DMA and tensile tests. PA6-NC had higher stiffness than

Table 1
Tensile data of PA6 and PA6-NC

Material	Thickness (mm)	E-modul (MPa)	σ_y (MPa)	σ_{max} (Mpa)	ε_y (%)	$\varepsilon_{failure}$ (%)	Work (J)
PA6	0.5	2610 ± 75	64.1 ± 1.0	64.0 ± 1.0	5.5 ± 2.6	100 ± 65	2.3 ± 1.4
	0.75	2580 ± 170	72.4 ± 0.7	72.0 ± 0.5	5.9 ± 0.1	156 ± 8	4.9 ± 0.3
	1.0	2730 ± 67	69.0 ± 1.0	70.0 ± 2.2	7.0 ± 2.2	230 ± 52	9.8 ± 2.3
	2.0	2450 ± 275	68.0 ± 0.7	68.4 ± 0.8	8.6 ± 0.8	238 ± 27	18.7 ± 2.2
PA6-NC	0.5	4730 ± 170	90.0 ± 1.3	90.0 ± 1.2	3.9 ± 0.9	27 ± 9	1.0 ± 0.3
	0.75	4420 ± 177	93.0 ± 1.3	93.4 ± 1.3	4.2 ± 0.2	34 ± 6	1.4 ± 0.3
	1.0	4160 ± 56	84.0 ± 0.7	84.5 ± 0.7	6.7 ± 0.1	49 ± 37	2.7 ± 2.0
	2.0	3750 ± 87	78.0 ± 0.2	78.0 ± 0.2	6.2 ± 0.2	39 ± 4	3.0 ± 0.3

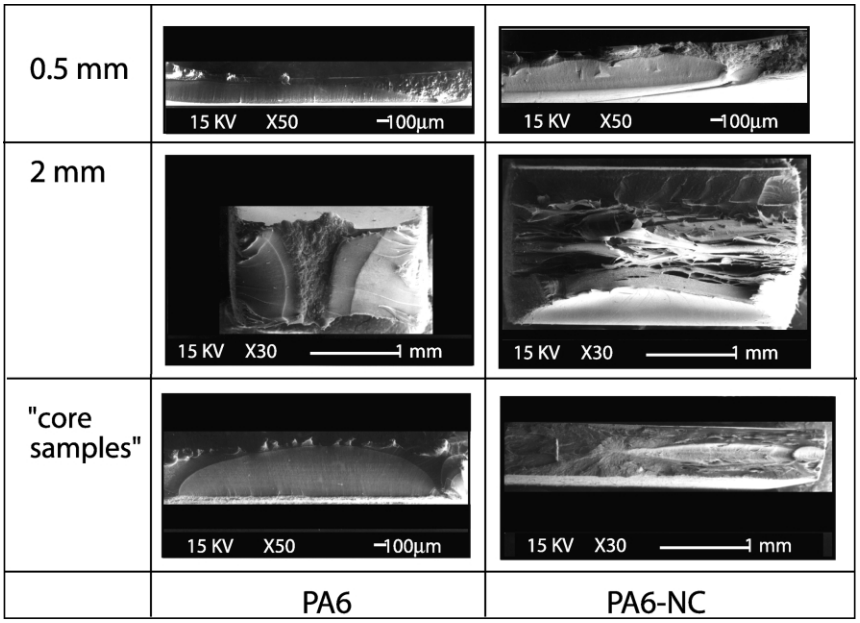

Fig. 6. SEM micrographs of selected PA6 and PA6-NC tensile fracture surfaces.

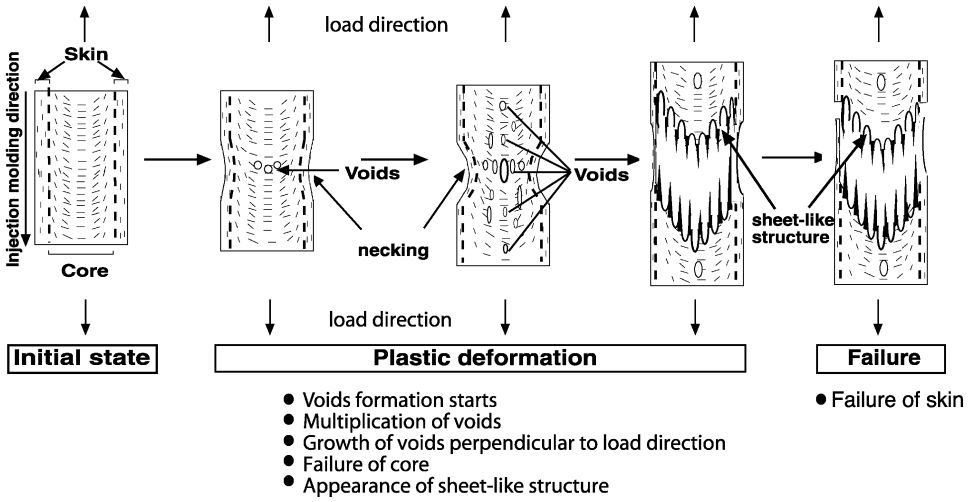

Fig. 7. Proposed micromechanical model of the fracture behavior of thick PA6-NC samples.

pure PA6, demonstrating the reinforcement caused by the layered silicates.

A skin-core effect was observed in PA6-NC under the processing conditions used. Thin samples of PA6-NC (0.5 mm) with a higher contribution of skin had the highest stiffness and strength and the tensile fracture surface was flat, reflecting fast crack propagation. Thicker samples (2 mm) with a higher contribution of core had a lower stiffness and strength and the fracture surface showed a flat surface in the skin and a sheet-like pattern in the core. This sheet-pattern formation can be explained as the result of multi-voiding due to stress concentrations in the core; the voids grew in the direction of the load, forming the sheets assisted by the skin that fails last.

In a complementary work that will be published elsewhere [32], the effects of layered silicates on the crystals and lamellae orientation across the thickness of the samples will be reported.

Acknowledgements

We want to thank the DFG (Deutsche Forschungsgemeinschaft) SFB 371 for the financial support of this work, as well as the BASF AG for the fabrication and supply of the studied samples, especially Dr Freddy Gruber and Dr Falko Ramsteiner for the useful commentaries and discussions.

References

[1] Knudson Jr. MI, Jones TR. US Patent 5160454.
[2] Farrow TC, Rasmussen CA, Menking WR, Durham DH, Carrol PW. US Patent 6036765.
[3] Gonzales A, Nichols KL, Powell CE, Thill BP. WO 9730950.
[4] Lan T, Kaviratna PD, Pinnavaia TJ. Chem Mater 1995;7:2144–50.
[5] Shi H, Lan T, Pinnavaia T. Chem Mater 1996;8:1584–7.
[6] Okada A, Kawakado M, Kurauchi N, Kamigado N. JP 62252426.
[7] Usuki A, Kojima Y, Kawasumi M, Okada A, Fukushima Y, Kurauchi T, Kamigaito O. J Mater Res 1993;8(5):1179–85.
[8] Maxfield M, Shacklette LW, Baughman RH, Christiani BR. EP 598836B1.
[9] Vaia RA, Tse OK, Giannelis EP. WO 9514733.
[10] Korbee RA, Van Geenen AA. WO 9929767.
[11] Togawa K, Nishimura T, Kumaki J. JP 11343410.
[12] Liu L, Qi Z, Zhu X. J Appl Polym Sci 1999;71:1133–8.
[13] Giannelis E. Adv Mater 1996;8(1):29–35.
[14] Burnside SD, Giannelis EP. Chem Mater 1995;7:1597–600.
[15] Gilman JW. Appl Clay Sci 1999;15:31–49.
[16] Gilman JW, Kashiwagi T, Lomakin S, Giannelis EP, Manias E, Lichtenhan JD, Jones P. Nanocomposites: radiative gasification and vinyl polymer flammability. Proceedings of the Sixth European Meeting on Fire Retardancy of Polymeric Materials (FRPM'97), France: University of Lille; 1997. p. 203–21.
[17] Kojima Y, Usuki A, Kawasumi M, Okada A, Kurauchi T, Kamigaito O. J Polym Sci Part A: Polym Chem 1993;31:1755–8.
[18] Kojima Y, Usuki A, Kawasumi M, Okada A, Fukushima Y, Kurauchi T, Kamigaito O. J Mater Res 1993;6:1185–9.
[19] Krishnamoorti R, Giannelis E. Macromolecules 1997;30:4097–102.
[20] Yamashita A, Takahara A, Kajiyama T. Compos Interfaces 1999;6(3):247–58.
[21] Medellin-Rodriguez F, Burger C, Hsiao B, Chu B, Vaia B, Phillips S. Polymer 2001;42(21):9015–23.
[22] Lincoln D, Vaia R, Wang Z, Hsiao B, Krishnamoorti R. Polymer 2001;42(25):9975–85.
[23] Vanderhart D, Asano A, Gilman J. Chem Mater 2001;13(10):3796–809.
[24] Akkapeddi M. Antec'99 Conference Proceedings, New York City; May 2–6 1999. p. 1619–22.
[25] Fukuda H, Kawata K. Fibre Sci Technol 1974;7:207–22.
[26] Robinson I, Robinson J. J Mater Sci 1994;29:4663–77.
[27] Reinsch V, Rebenfeld L. Polym Compos 1992;13(5):353–60.
[28] Deporter J, Baird D. Polym Compos 1993;14(3):201–13.
[29] Ehrenstein G, Wurmb R. Die Angew Makromol Chem 1977;60/61(851):157–214.
[30] Hegler R, Altstädt V, Ehrenstein G, Menig G, Scharschmidt J, Weber G. Kunststoffe 1986;76(9):766–71.
[31] Michler G. Kunststoff-mikromechanik. Morphologie, deformations- und bruchmechanismen. München: Carl Hanser Verlag; 1992.
[32] Yebra-Rodriguez A, Uribe-Arocha P, Mehler C, Puskas J, Altstädt V. In preparation.